JCI The Journal of Clinical Investigation

Autocrine lysophosphatidic acid signaling activates β-catenin and promotes lung allograft fibrosis

Pengxiu Cao, … , Eric R. Fearon, Vibha N. Lama

J Clin Invest. 2017;127(4):1517-1530. https://doi.org/10.1172/JCI88896.

Research Article **Cell biology** **Transplantation**

Tissue fibrosis is the primary cause of long-term graft failure after organ transplantation. In lung allografts, progressive terminal airway fibrosis leads to an irreversible decline in lung function termed bronchiolitis obliterans syndrome (BOS). Here, we have identified an autocrine pathway linking nuclear factor of activated T cells 2 (NFAT1), autotaxin (ATX), lysophosphatidic acid (LPA), and β-catenin that contributes to progression of fibrosis in lung allografts. Mesenchymal cells (MCs) derived from fibrotic lung allografts (BOS MCs) demonstrated constitutive nuclear β-catenin expression that was dependent on autocrine ATX secretion and LPA signaling. We found that *NFAT1* upstream of *ATX* regulated expression of ATX as well as β-catenin. Silencing *NFAT1* in BOS MCs suppressed *ATX* expression, and sustained overexpression of *NFAT1* increased *ATX* expression and activity in non-fibrotic MCs. LPA signaling induced NFAT1 nuclear translocation, suggesting that autocrine LPA synthesis promotes NFAT1 transcriptional activation and ATX secretion in a positive feedback loop. In an in vivo mouse orthotopic lung transplant model of BOS, antagonism of the LPA receptor (LPA1) or ATX inhibition decreased allograft fibrosis and was associated with lower active β-catenin and dephosphorylated NFAT1 expression. Lung allografts from β-catenin reporter mice demonstrated reduced β-catenin transcriptional activation in the presence of LPA1 antagonist, confirming an in vivo role for LPA signaling in β-catenin activation.

Autocrine lysophosphatidic acid signaling activates β-catenin and promotes lung allograft fibrosis

Pengxiu Cao,[1] Yoshiro Aoki,[1] Linda Badri,[1] Natalie M. Walker,[1] Casey M. Manning,[1] Amir Lagstein,[2] Eric R. Fearon,[3] and Vibha N. Lama[1]

[1]Division of Pulmonary and Critical Care Medicine, Department of Internal Medicine, University of Michigan Health System, [2]Department of Pathology, University of Michigan, and [3]Department of Human Genetics, University of Michigan Health System, Ann Arbor, Michigan, USA.

Tissue fibrosis is the primary cause of long-term graft failure after organ transplantation. In lung allografts, progressive terminal airway fibrosis leads to an irreversible decline in lung function termed bronchiolitis obliterans syndrome (BOS). Here, we have identified an autocrine pathway linking nuclear factor of activated T cells 2 (NFAT1), autotaxin (ATX), lysophosphatidic acid (LPA), and β-catenin that contributes to progression of fibrosis in lung allografts. Mesenchymal cells (MCs) derived from fibrotic lung allografts (BOS MCs) demonstrated constitutive nuclear β-catenin expression that was dependent on autocrine ATX secretion and LPA signaling. We found that *NFAT1* upstream of *ATX* regulated expression of ATX as well as β-catenin. Silencing *NFAT1* in BOS MCs suppressed *ATX* expression, and sustained overexpression of *NFAT1* increased *ATX* expression and activity in non-fibrotic MCs. LPA signaling induced NFAT1 nuclear translocation, suggesting that autocrine LPA synthesis promotes NFAT1 transcriptional activation and ATX secretion in a positive feedback loop. In an in vivo mouse orthotopic lung transplant model of BOS, antagonism of the LPA receptor (LPA1) or ATX inhibition decreased allograft fibrosis and was associated with lower active β-catenin and dephosphorylated NFAT1 expression. Lung allografts from β-catenin reporter mice demonstrated reduced β-catenin transcriptional activation in the presence of LPA1 antagonist, confirming an in vivo role for LPA signaling in β-catenin activation.

Introduction

Fibrogenesis in the transplanted organ is the predominant cause of allograft failure and death across all solid organs. By 5 years after transplantation, 50% of lung transplant recipients develop chronic graft failure, with evidence of a progressive obstructive ventilatory defect termed bronchiolitis obliterans syndrome (BOS) arising from fibrotic obliteration of the small airways or bronchiolitis obliterans (BO) (1). Graft injury arising from various mechanisms, including allo- and autoimmune insults, microvascular ischemia, and infectious agents, is presumed to drive mesenchymal cell infiltration and collagen deposition, which characterize a failing graft. While previously considered as rather generic effector cells, mesenchymal cells (MCs) are now being increasingly recognized for their organ-specific transcriptome (2). We have demonstrated that graft-resident lung-specific mesenchymal stromal cells play a pathogenic role in BOS, with evidence for their presence in fibrotic lesions and their mobilization preceding BOS (2–4). A stable fibrotic phenotype marked by increased matrix synthetic function is noted in MCs isolated from BOS lungs (4). Persistent activation of MCs even after these cells are removed from their local milieu is also seen in other fibrotic diseases and provides an explanation for the progressive nature of fibrosis (5, 6). However, although MCs are increasingly recognized for their secretory functions (7), the mechanisms of autocrine regulation of MC fibrotic differentiation remain to be elucidated.

β-Catenin, an integral cell-cell adhesion adaptor protein and a transcriptional coregulator, has been recently identified to be important in MC activation (8–12). β-Catenin stabilization in MCs in transgenic mice is sufficient to promote spontaneous fibrotic lesions (9). Transient β-catenin activation in MCs marks normal wound healing; persistent β-catenin activation is noted in MCs of hyperplastic skin lesions and other human fibrotic diseases (8, 10). However, mechanisms of β-catenin regulation in MCs in tissue fibrosis have not been identified. While the best-known activator of β-catenin is WNT1, recent studies indicate a role for various other ligands and receptors, including GPCRs, in activation of the β-catenin pathway (13, 14). We have previously demonstrated that lysophosphatidic acid (LPA) acting via ligation of LPA receptor 1 (LPA1) induces cytoplasmic accumulation, nuclear translocation, and transcriptional activation of β-catenin in human lung-resident mesenchymal stromal cells (15). LPA, a bioactive lipid mediator produced from extracellular lysophosphatidylcholine by autotaxin (ATX), a secreted lysophospholipase D, has been shown to have an important role in tissue fibrosis (16–19). However, it is not known whether LPA acts as a ligand for β-catenin activation in regulating tissue fibrosis and what role it plays in lung allograft fibrogenesis.

Here, we investigate the upstream signaling nexus that induces persistent β-catenin activation and the fibrotic phenotype of MCs in BOS. We identify an autocrine loop linking nuclear factor of activated T cells 2 (NFAT1) to β-catenin via NFAT1 regulation of ATX expression and subsequent LPA1 signaling. Furthermore, we ascertain the in vivo relevance of this signaling axis in allograft fibrogene-

Authorship note: P.X. Cao and Y. Aoki contributed equally to this work.
Conflict of interest: The authors have declared that no conflict of interest exists.
Submitted: June 1, 2016; **Accepted:** January 5, 2017.
Reference information: *J Clin Invest*. 2017;127(4):1517–1530.
https://doi.org/10.1172/JCI88896.

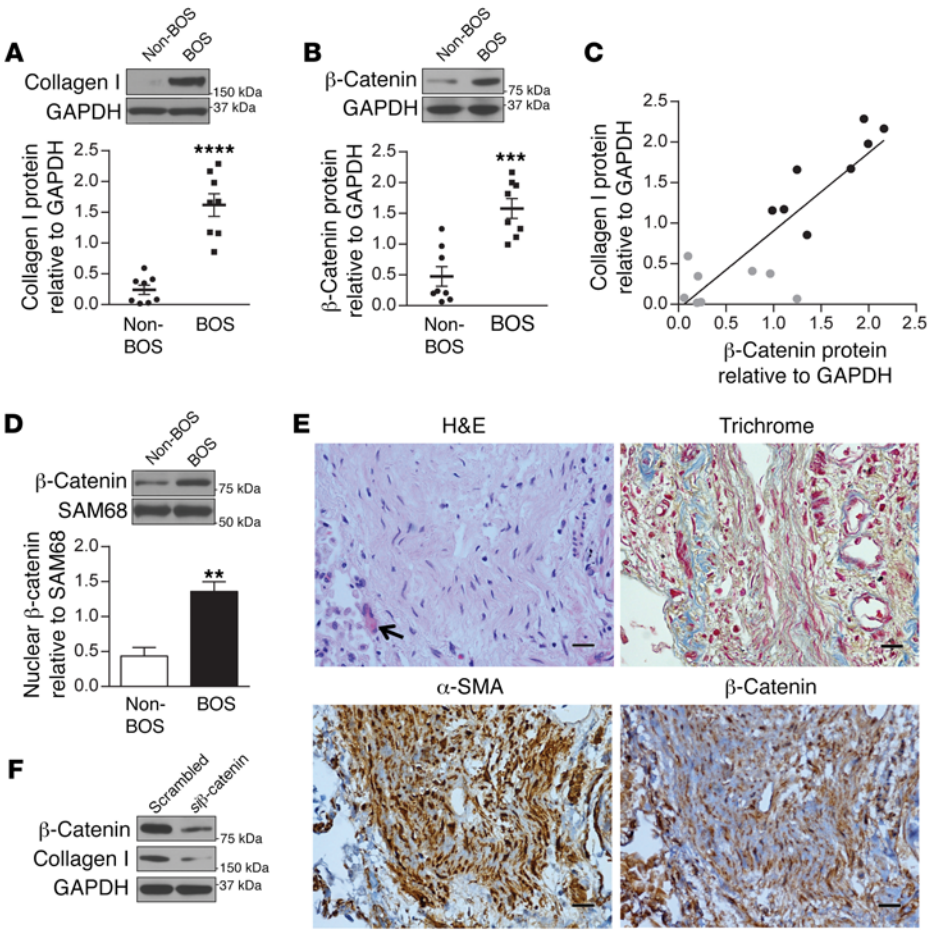

Figure 1. Increased MC β-catenin expression in fibrotic human lung allografts. (**A** and **B**) Collagen I and β-catenin protein levels in MCs derived from lung allografts with and without BOS were analyzed by immunoblotting. Mean ± SEM (n = 8/group). P values were obtained by unpaired t test. The collagen I antibody recognizes both chains of α1 and α2. (**C**) Correlation of total β-catenin and collagen I protein expression in individual patient-derived MCs is shown ($P < 0.0001$ determined by 2-tailed test; $r^2 = 0.7310$ obtained by correlation). Non-BOS MCs (gray dots, n = 8), BOS MCs (black dots, n = 8). (**D**) Nuclear fraction of β-catenin in BOS and non-BOS MCs was measured by immunoblotting. Mean ± SEM (n = 5/group) with unpaired t test. (**E**) Representative images of β-catenin and α-SMA immunohistochemical staining of histological sections demonstrating BO. H&E and trichrome staining demonstrate a tangentially cut, completely obliterated bronchus. Myofibroblasts in the fibrous plug in the lumen of the bronchus are recognized by positive α-SMA immunohistochemical staining (brown DAB). Overlapping of β-catenin staining with hematoxylin blue nuclear stains was noted in these MCs. Scale bars: 20 μm. (**F**) Expression of β-catenin contributes to fibrotic functions of BOS MCs. BOS MCs were transfected with β-catenin siRNA or scrambled siRNA, and protein expression was measured by immunoblotting (n = 5/group). $^{**}P < 0.01$, $^{***}P < 0.001$, $^{****}P < 0.0001$.

sis in a murine lung transplant model of BO. Together, these studies uncover an interaction of NFAT1 and the β-catenin pathway, validate LPA as an in vivo activator of β-catenin–dependent transcription during allograft fibrogenesis, and suggest a potential therapeutic role for LPA1 antagonists and ATX inhibition in BOS.

Results

β-Catenin stabilization in BOS MCs and its profibrotic functions. We have previously demonstrated that MCs derived from fibrotic human lung allografts have an altered profibrotic phenotype, with increased expression of matrix proteins such as collagen I (4). To investigate whether β-catenin signaling is activated in MCs during allograft fibrogenesis, we first compared β-catenin protein expression in MCs isolated from lung allografts of patients with evidence of BOS (BOS MCs) and those isolated from BOS-free controls matched by time after lung transplant (non-BOS MCs). BOS MCs demonstrated significantly higher collagen I and β-catenin protein expression in the whole cell lysates as compared with non-BOS MCs ($P < 0.0001$ and $P < 0.001$, respectively) (Figure 1, A and B). A significant positive correlation was noted between the total β-catenin expression and collagen I expression of MCs (Figure 1C, $P < 0.0001$; $r^2 = 0.7310$). β-Catenin expression was also higher in the nuclear fraction of BOS MCs compared with non-BOS cells (Figure 1D). Immunocytochemistry of β-catenin confirmed upregulation and increased nuclear localization of β-catenin in BOS MCs compared with non-BOS MCs (Supplemental Figure 1; supplemental material available online with this article; https://doi.org/10.1172/JCI88896DS1). Next, β-catenin expression in situ in BO lesions in human lung allografts was examined by immunohistochemical staining. β-Catenin expression was noted in the nuclei of MCs in fibrotic airways (Figure 1E). To determine whether β-catenin contributes to the maintenance of a fibrotic phenotype in BOS MCs, we utilized β-catenin siRNA, and a decrease in collagen I protein expression was noted, suggesting that β-catenin is critical for the maintenance of fibrotic functions of BOS MCs (Figure 1F).

Autocrine ATX/LPA/LPA1 signaling axis contributes to β-catenin stabilization and collagen expression in BOS MCs. The free pool of β-catenin that is active in transcription is tightly regulated by its phosphorylation, ubiquitination, and proteasomal degradation (20). Glycogen synthase kinase 3β (GSK-3β) interacts with adenomatous polyposis coli and axin proteins to form a destruction complex that phosphorylates β-catenin and makes it a target for proteasome-mediated degradation. We have previously shown that in human lung MCs, exogenous LPA via LPA1 ligation leads to GSK-3β phosphorylation, which inhibits β-catenin degradation and leads to β-catenin pathway activation (15). Comparison of BOS and non-BOS MCs demonstrated increased pGSK-3β expression in BOS cells; pGSK-3β phosphorylation was decreased when cells were transfected with LPA1 siRNA (Figure 2, A and B). More significantly, LPA1 silencing was found to robustly inhibit collagen I and β-catenin protein expression in BOS MCs (Figure 2C), suggesting a role for endogenous LPA in regulating β-catenin sta-

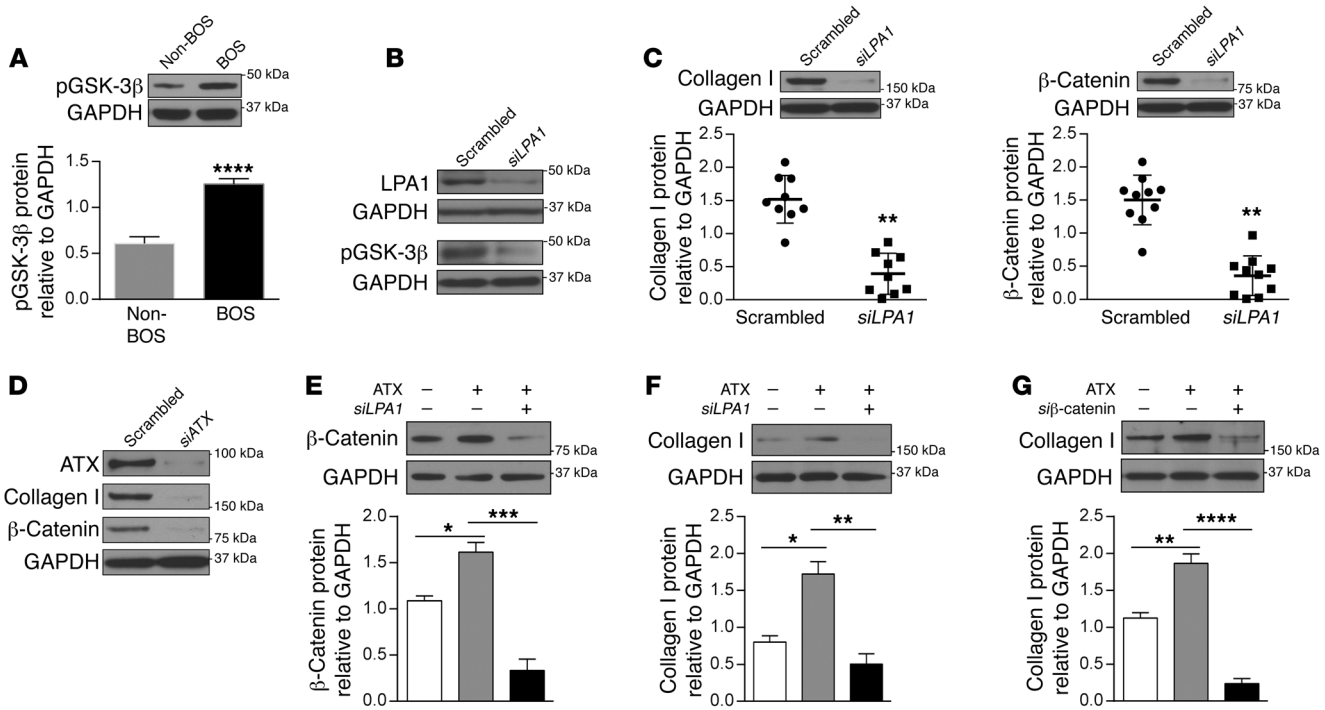

Figure 2. Function of the ATX/LPA/LPA1 signaling axis in β-catenin stabilization and collagen I induction in MCs. (**A**) Phospho–GSK-3β (Ser9) protein expression in BOS and non-BOS MCs as measured by immunoblotting. Mean ± SEM (n = 5 for non-BOS MCs and 6 for BOS MCs with unpaired t test). (**B** and **C**) BOS MCs were transfected with *LPA1* siRNA or scrambled siRNA and analyzed by immunoblotting. Representative immunoblots shown are from the same biological sample. Blots of collagen I and β-catenin from one membrane and hence the same loading control (GAPDH) blot are shown. Quantitative analysis demonstrates the effect of *LPA1* silencing on collagen I (n = 9) and β-catenin (n = 10) protein expression in MCs derived from individual patients with BOS (mean ± SEM, paired t test). (**D**) BOS MCs were transfected with *siATX* or scrambled siRNA, and protein expression was analyzed by immunoblotting (n = 4). (**E**–**G**) Non-BOS MCs were treated with recombinant ATX (100 ng/ml, 24 hours). In the indicated conditions, cells were transfected with *LPA1* or β-catenin siRNA before ATX treatment. Mean ± SEM (n = 5/group for **E** and **F**, and n = 4/group for **G** with ANOVA). Data were similar in 3 independent experiments. $^*P < 0.05$, $^{**}P < 0.01$, $^{***}P < 0.001$, $^{****}P < 0.0001$.

bilization and fibrotic differentiation. As LPA is predominantly synthesized by actions of ATX (21, 22), LPA generation in MCs was targeted next by inhibiting expression of ATX. A substantial decrease in both β-catenin and collagen I protein expression was noted in BOS MCs transfected with *ATX* siRNA (Figure 2D). This ATX/LPA/LPA1/β-catenin signaling axis of MC activation was confirmed by studying the effect of exogenous recombinant ATX on non-BOS MCs. Recombinant ATX increased β-catenin protein expression in MCs from non-BOS lung allografts, and this response was blocked by *LPA1* siRNA (Figure 2E). Additionally, induction of collagen I by recombinant ATX was noted to be dependent on LPA1 and β-catenin signaling, as demonstrated by the failure of ATX to induce an increase in collagen I in non-BOS MCs in the presence of *LPA1* and β-catenin siRNA (Figure 2, F and G).

Next, we compared ATX expression and activity in BOS versus non-BOS MCs. ATX protein expression in whole cell lysates was noted to be significantly higher in BOS MCs (Figure 3A). ATX was also quantitated by ELISA in MC supernatants. BOS MCs were found to secrete approximately 4-fold-higher levels of ATX than non-BOS MCs (Figure 3B). ATX activity was measured in the cell supernatant by utilizing a fluorogenic phospholipid ATX substrate, and increased ATX activity was confirmed in the supernatant from BOS as compared with non-BOS MCs (Figure 3C). ATX expression in MCs in situ was studied by immunohistochemical staining of human BO lesions, where intense staining with ATX antibody was noted in MCs expressing α–smooth muscle actin (α-SMA) (Figure 3D).

Autocrine LPA synthesis and signaling are requisite for establishing fibrotic lesions of BOS MCs after adoptive transfer. Adaptive transfer experiments were performed to confirm the role of the ATX/LPA/LPA1 axis in regulating fibrotic functions of human BOS MCs in vivo. DsRed lentivirus–labeled non-BOS and BOS MCs (0.5×10^6) were injected intratracheally into the lungs of Beige/Nude/XID triple-immunodeficient mice. Lungs were examined on day 45 by immunofluorescence imaging and immunohistochemistry. As shown in Figure 4A, non-BOS MCs demonstrated engraftment as single cells in alveolar corners, as previously described (23). However, BOS MCs demonstrated formation of cellular clusters and caused architectural distortion (Figure 4A), as has been demonstrated before with MCs derived from other fibrotic lung diseases (24). The interstitial localization of the cellular clusters was established by confocal microscopy (Figure 4B). These fibrotic foci caused architectural distortion and were marked by collagen and α-SMA expression (Figure 4, C and D). To determine whether the ATX/LPA/LPA1 signaling pathway is important for BOS MCs to establish fibrotic lesions in an vivo environment, we infected DsRed-labeled human BOS MCs with lentiviruses expressing shRNA targeting *LPA1* or *ATX*, or a control scrambled vector, pLKO.1, before intratracheal administration into

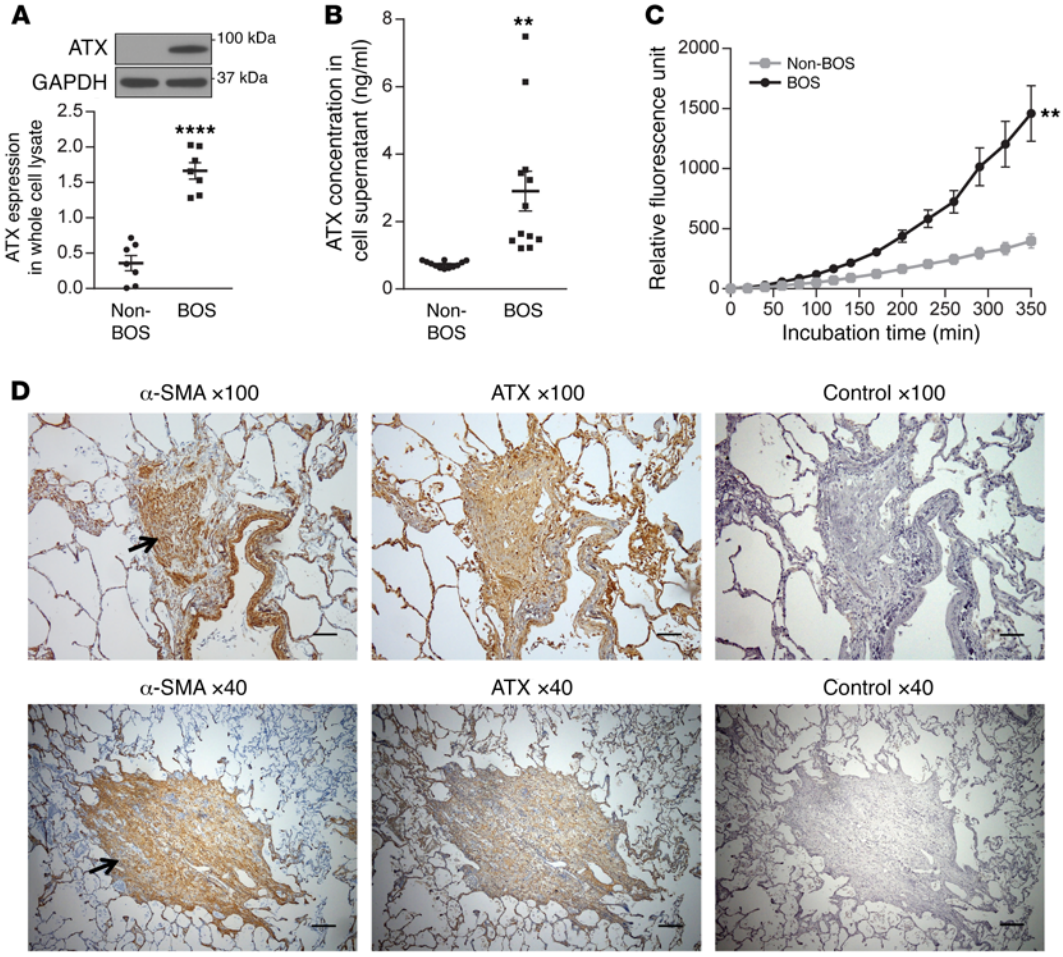

Figure 3. **Increased ATX expression and activity in BOS MCs.** (**A**) Basal ATX expression in BOS and non-BOS MCs was measured by immunoblotting in whole cell lysates. Mean ± SEM (n = 7/group) with unpaired t test. (**B**) ATX expression in cell supernatant (24-hour collection) was quantitated by ELISA. Mean ± SEM (n = 12/group) with unpaired t test. (**C**) Cell supernatant collected after 72 hours of incubation from BOS and non-BOS MCs was concentrated, and ATX activity was assayed using the fluorogenic phospholipid ATX substrate FS-3 (n = 4 for BOS MCs and 5 for non-BOS MCs with ANOVA). Data were repeated in 3 independent experiments. Mean ± SEM. $^{**}P < 0.01$, $^{****}P < 0.0001$. (**D**). Serial sections from lung allografts of patients with BOS collected at autopsy were analyzed by immunohistochemistry for ATX or α-SMA and counterstained with hematoxylin. Two separate areas with completely obliterated airways are shown in the top and bottom panels. Arrows indicated the obliterated bronchi. Scale bars: 80 μm for ×100 images and 200 μm for ×40 images.

murine lungs. Both *LPA1* silencing and *ATX* silencing via shRNA approaches in BOS MCs prevented establishment of fibroproliferative human MC lesions in the recipient lung (Figure 4E). Quantitative analysis, performed by counting cellular clusters (≥3 cells) of human MCs per high-power field in murine lung sections, confirmed these findings (Figure 4E).

Regulation of ATX by NFAT1 in lung MCs. Higher expression of ATX in BOS MCs led us to investigate the mechanisms regulating ATX expression in these cells. Transcription of the ATX-encoding gene ectonucleotide pyrophosphatase/phosphodiesterase 2 (*ENPP2*) has been shown to be under the control of transcription factor NFAT1 (25, 26). BOS MCs were noted to demonstrate increased NFAT1 expression in whole cell and nuclear lysates (Figure 5, A and B). *NFAT1* siRNA significantly inhibited ATX activity in cell supernatant from BOS MCs (Figure 5C). BOS MCs transfected with *NFAT1* siRNA also demonstrated significantly decreased ATX protein expression as well as β-catenin and collagen I protein expression (Figure 5D). To further confirm the ability of *NFAT1* to regulate *ATX* expression and its activity in MCs, we overexpressed constitutively active *NFAT1* in non-BOS MCs. NFAT1 overexpression in non-BOS MCs was associated with a marked increase in ATX expression (Figure 5E). Total and active β-catenin and collagen I were also induced by NFAT1 overexpression. ATX activity in non-BOS MCs, which was very low at baseline, was significantly increased in the presence of constitutively active NFAT1 (Figure 5F). At the transcriptional level, a roughly 5-fold increase in *ATX* and collagen type I alpha 1 chain (*COL1A1*) mRNA was noted in non-BOS MCs with *NFAT1* overexpression (Figure 5G). Expression of *AXIN2*, a β-catenin target gene, increased roughly 16-fold in *NFAT1*-overexpressing cells, demonstrating *NFAT1* regulation of β-catenin transcription activity (Figure 5G).

Autocrine loop of NFAT1 and ATX regulation by LPA. LPA is known to increase intracellular free Ca^{2+} concentration ($[Ca^{2+}]_i$), which has been linked to NFAT activation and nuclear translocation (27–29). To investigate the possible involvement of LPA in mediating NFAT1 nuclear translocalization in lung MCs,

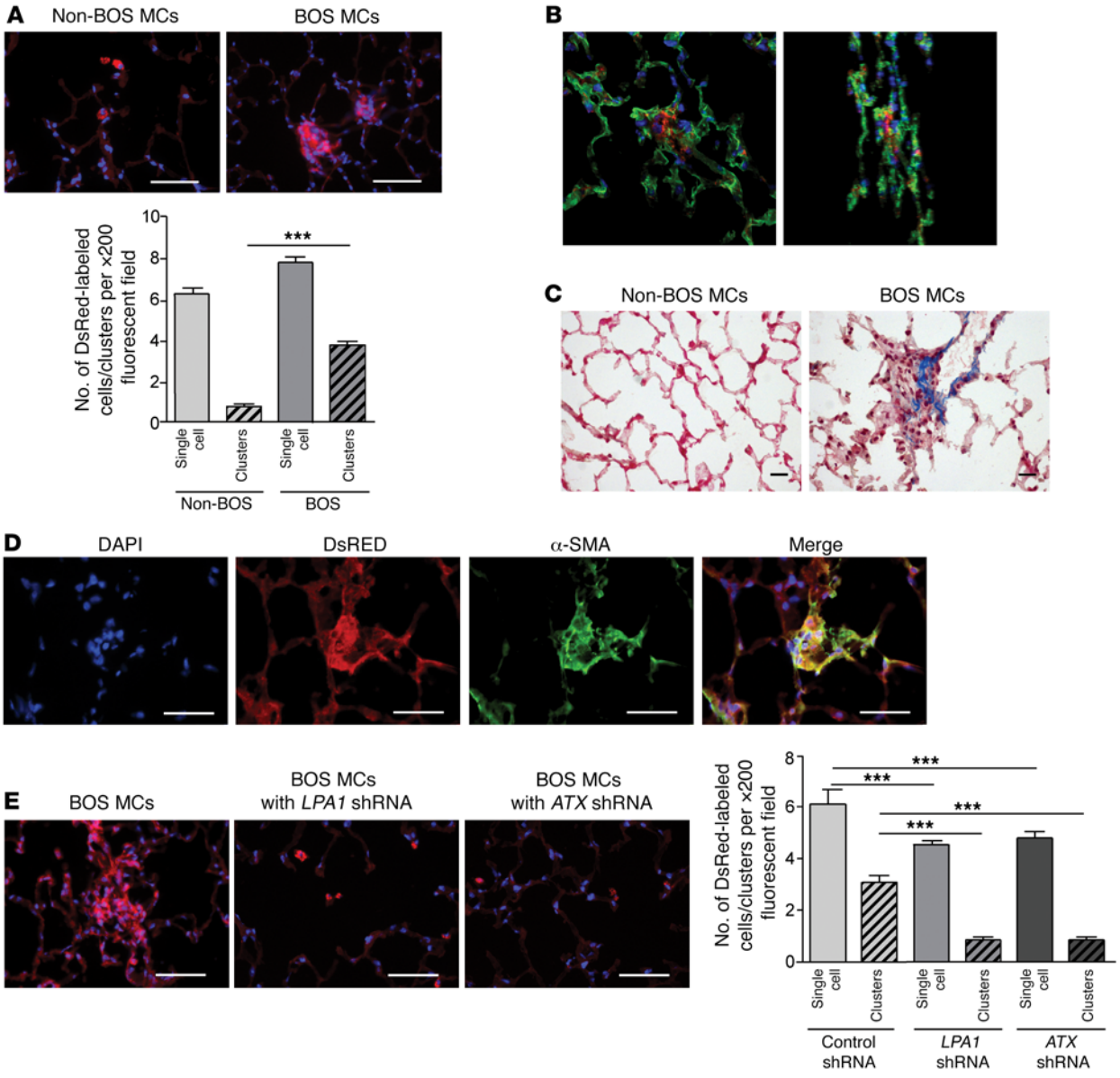

Figure 4. **In vivo fibrotic behavior of human BOS MCs after adoptive transfer demonstrates dependence on intact ATX/LPA1 signaling.** (**A**) BOS MCs establish fibrotic lesions in vivo after adaptive transfer. MCs obtained from normal and fibrotic human lung allograft (non-BOS MCs and BOS MCs) were infected with DsRed lentivirus and adoptively transferred via intratracheal administration into lungs of immunodeficient (Beige/Nude/XID) mice. Lungs were harvested on day 45 after administration of cells and stained with DAPI. Lower panel shows quantitative analysis of single cells or cell clusters (>3 adjacent cells) of human MCs in murine lung sections. Nucleated red fluorescent cells were quantitated under ×200 magnification in 12 fields per slide. Mean ± SEM with ANOVA (n = 4 for non-BOS MCs and 10 for BOS MCs). Scale bars: 50 μm. (**B**) Confocal microscopy demonstrating interstitial localization of human BOS MCs engrafted in immunodeficient mouse lungs. Epithelia were stained green by cytokeratin immunofluorescence staining (MAB3412, Millipore). Images of z-projections from two different rotation angles are shown. (**C**) Trichrome staining images of immunodeficient mouse lungs intratracheally transferred with non-BOS or BOS MCs. Scale bars: 20 μm. (**D**) Characterization of fibrotic lesions induced by adoptive transfer of BOS MCs into immunodeficient mouse lungs. Positive immunofluorescence staining with α-SMA antibody (M0851, Dako) was noted in DsRed fluorescent human BOS MC clusters. Scale bars: 50 μm. (**E**) Endogenous LPA synthesis and signaling are requisite for establishing fibrotic lesions of BO MCs after adoptive transfer. DsRed-labeled BOS MCs were infected with lentivirus containing the silencing control vector, *LPA1* shRNA, or *ATX* shRNA and then were adoptively transferred into immunodeficient mice. BOS MCs infected with *LPA1* or *ATX* shRNA–expressing lentivirus failed to form fibrotic lesions. Right panel shows quantitative analysis. Mean ± SEM (n = 3/group with ANOVA). Scale bars: 50 μm. ***$P < 0.001$.

we transfected non-BOS MCs with a plasmid encoding a GFP-NFAT1 fusion protein and treated them with LPA. Immunofluorescence imaging demonstrated increased nuclear localization of GFP in the presence of LPA (Figure 6A). Immunoblot studies showed a roughly 6-fold increase in NFAT1 nuclear protein expression at 15 minutes after LPA treatment (Figure 6B). LPA treatment of non-BOS MCs was also noted to induce an increase in ATX protein expression at 24 and 48 hours (Figure 6C). Higher ATX activity was noted in the supernatant of MCs treated with LPA (Figure 6D). To determine whether LPA-induced ATX

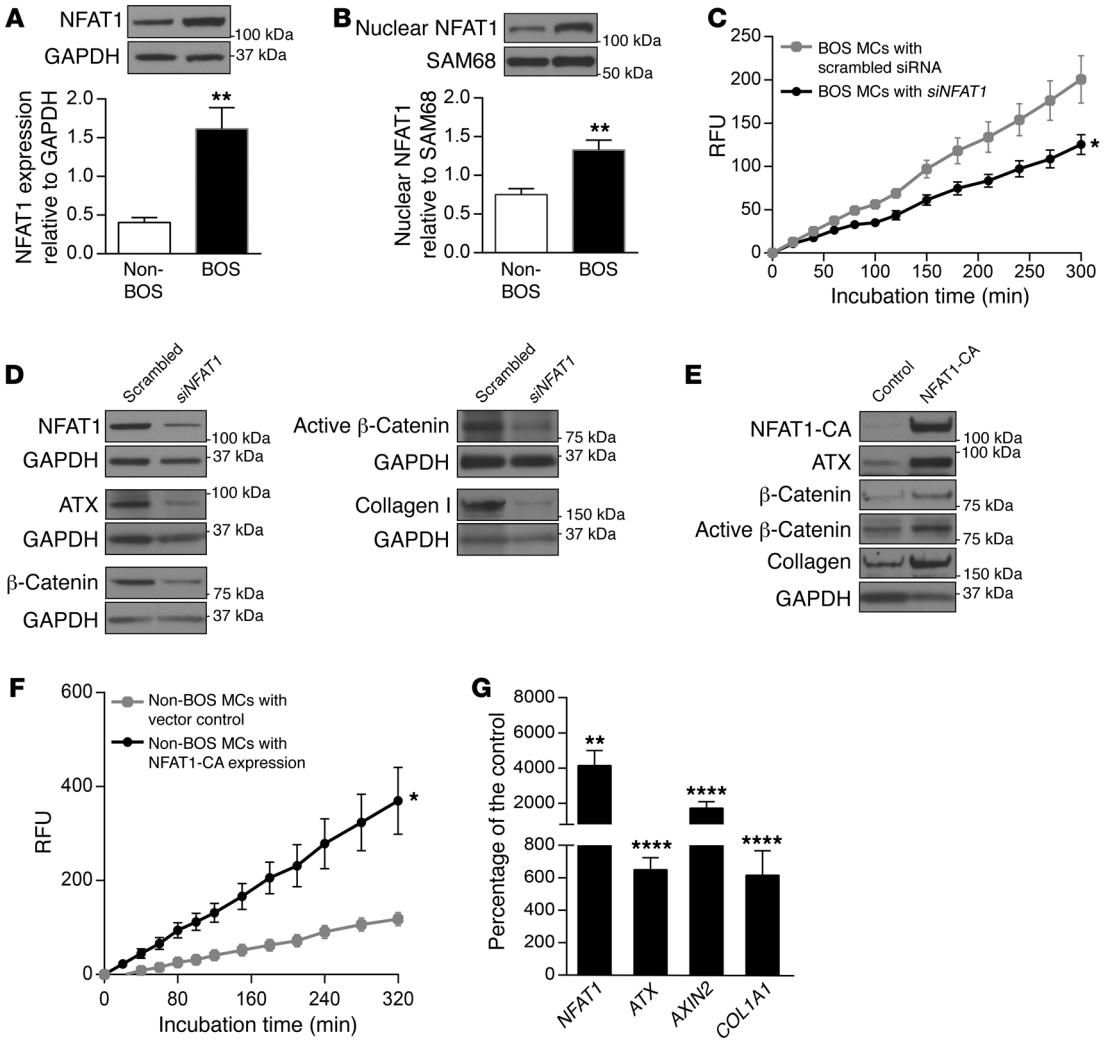

Figure 5. NFAT1 regulates *ATX*, β-catenin, and collagen I expression in lung MCs. (**A** and **B**) Expression of NFAT1 protein in whole cell lysate (n = 4/group) and nuclear extract (n = 5–6/group) in BOS and non-BOS MCs measured by immunoblotting with unpaired t test. (**C**) ATX activity was measured in concentrated cell supernatant from BOS MCs transfected with *NFAT1*-specific or scrambled siRNA (n = 4/group with 2-way ANOVA). (**D**) BOS MCs were transfected with siRNAs for *NFAT1* or scrambled control, and protein expression of ATX, β-catenin, active β-catenin, and collagen I was analyzed by immunoblotting (n = 7/group). (**E**) Non-BOS MCs were infected with lentivirus expressing pLentilox-*NFAT1-CA*-IRES-Puro plasmid or DsRed-expressing vector control, and the indicated protein levels were examined in parallel gels (n = 6/group). NFAT1-CA, constitutively active NFAT1. (**F**) ATX activity in the cell supernatant from non-BOS MCs infected with lentivirus expressing NFAT1-CA was assayed (n = 3/group with 2-way ANOVA). (**G**) *NFAT1*, *ATX*, *AXIN2*, and *COL1A1* mRNA levels were assayed by real-time PCR in non-BOS MCs infected with lentivirus expressing NFAT1-CA. Mean ± SEM (n = 7–8/group) with paired t test. Experiments were repeated 3 times; $^*P < 0.05$, $^{**}P < 0.01$, $^{****}P < 0.0001$.

expression occurs via an NFAT1-dependent mechanism, we measured ATX activity in the presence of LPA in cells transfected with scrambled or *NFAT1* siRNA. ATX activity in LPA-treated cells was significant dampened by *NFAT1* silencing (Figure 6E), suggesting that LPA regulates ATX via its induction of NFAT1 activity. Next, to investigate whether endogenous LPA positively regulates ATX expression in an apparent feed-forward and autocrine manner in fibrotic MCs, the effect of interruption of LPA1 signaling on ATX expression was examined in BOS MCs. *LPA1* silencing decreased ATX expression at both the protein and mRNA ($P < 0.01$) level in BOS MCs (Figure 6, F and G). NFAT1 protein expression and *NFAT1* mRNA levels were also decreased with *LPA1* silencing (Figure 6, F and G). As expected, silencing of *ATX* did not affect LPA1 expression (Figure 6H).

Together these investigations of human lung allograft–derived MCs suggest an autocrine loop of MC activation, where ATX secretion and downstream LPA1 signaling act as an intermediary in tying NFAT1 to β-catenin activation. A schematic of the autocrine loop of NFAT1/ATX/LPA/LPA1/β-catenin signaling axis of MC activation suggested by these data and its proposed in vivo targeting is presented in Figure 6I.

LPA1 antagonism inhibits fibrogenesis in a murine orthotopic lung transplant model of BO. To further investigate the in vivo relevance of this proposed pathway in allograft fibrogenesis, we investigated the effect of LPA1 antagonism in an orthotopic murine lung transplant model of BO. We have recently characterized a robust whole lung transplant model of BO where transplantation of lung from an F_1 to a parent mouse (B6D2F1/J→DBA/2J) exhibits progressive

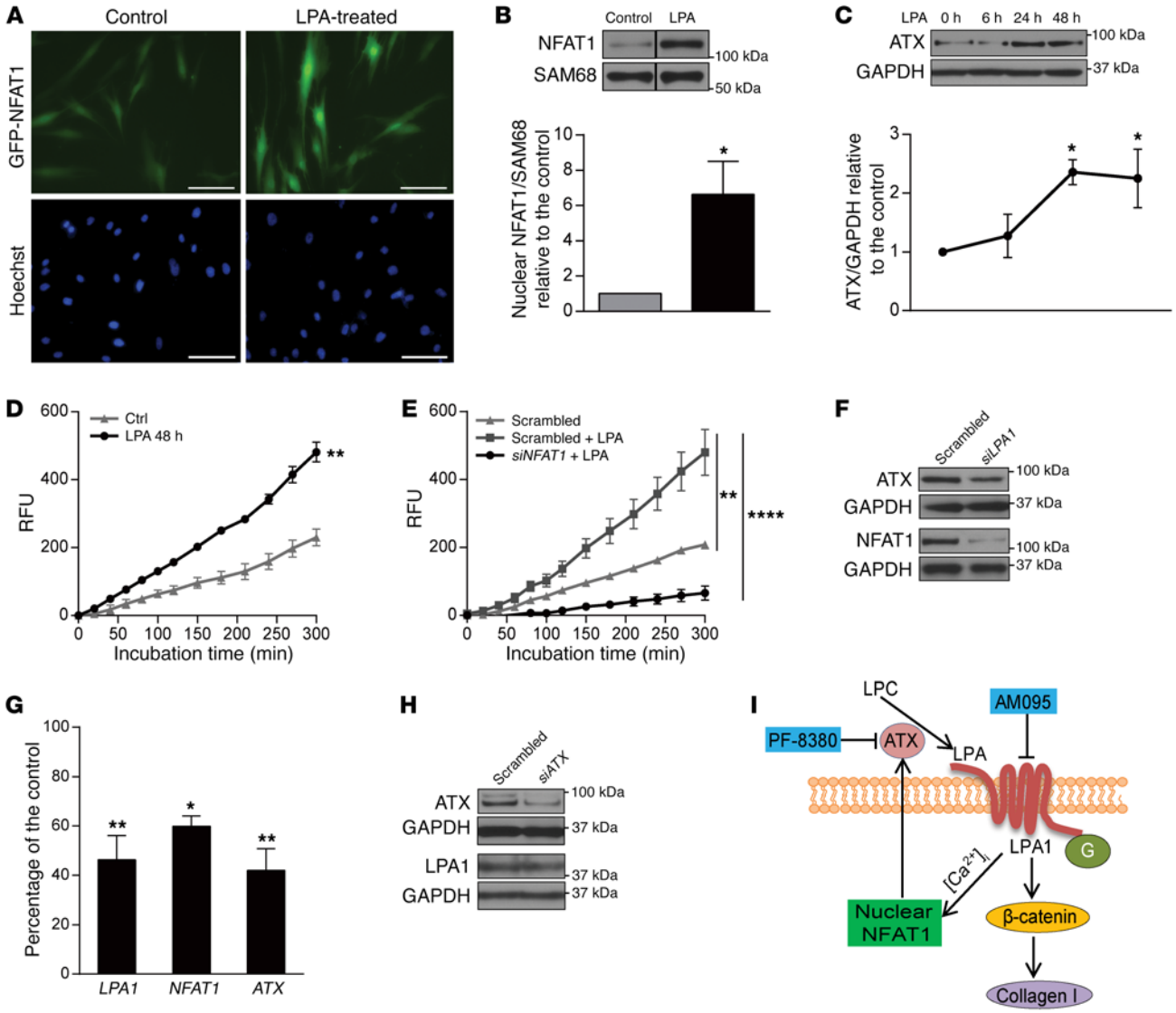

Figure 6. Autocrine loop of NFAT1 and ATX regulation by LPA. (**A**) Representative live cell imaging of non-BOS MCs expressing GFP-NFAT1 in the presence or absence of LPA (10 μM, 1 hour) (n = 5/group). Scale bars: 100 μm. (**B**) Non-BOS MCs were treated with LPA, and NFAT1 expression in nuclear extract was analyzed by immunoblotting. Lanes were run on the same gel but were noncontiguous, as indicated by the black lines. Mean ± SEM (n = 4/group with paired t test). (**C**) ATX expression in whole cell lysates of non-BOS MCs treated with LPA (10 μM) for varying time intervals. Mean ± SEM (n = 4/group with 1-way ANOVA). (**D**) ATX activity as measured in concentrated conditioned medium from non-BOS MCs cultured in the presence or absence (Ctrl) of LPA (n = 3/group with 2-way ANOVA). (**E**) Non-BOS MCs were transfected with *NFAT1* siRNA or scrambled siRNA and treated with LPA for 48 hours (10 μM). The ATX activity in concentrated cell supernatant is shown (n = 9/group with 2-way ANOVA). The results represent mean ± SEM from 2 independent experiments. (**F**) NFAT1 and ATX protein expression was analyzed by immunoblotting in BOS MCs transfected with siRNAs for *LPA1* or scrambled control (n = 5/group). (**G**) *LPA1*, *NFAT1*, and *ATX* mRNA expression was assayed by real-time PCR in BOS MCs transfected with *LPA1* siRNA or scrambled control siRNA. Mean ± SEM (n = 3–6/group with paired t test). Experiments were performed twice. (**H**) ATX and LPA1 expression in MCs transfected with *siATX* was assayed by immunoblotting with scrambled siRNA transfected MCs as control. Mean ± SEM (n = 8/group with paired t test). $^*P < 0.05$, $^{**}P < 0.01$, $^{****}P < 0.0001$. (**I**) Schematic model of the proposed pathway by which autocrine LPA production regulates MC activation. G, G proteins; AM095, LPA1 inhibitor; PF-8380, ATX inhibitor.

peribronchial fibrosis with high penetrance and reproducibility (30). To investigate the role of LPA1 signaling in allograft fibrogenesis, we treated lung allograft recipients with the LPA1 antagonist AM095 or vehicle administered twice daily by oral gavage starting on day 14. A dose of 30 mg/kg was utilized, as it has been shown to attain mouse plasma AM095 concentrations that were consistently greater than the IC_{50} for LPA1 (16). Two treatment durations, from days 14 to 28 and days 14 to 40 after transplantation, were used, and all graft lungs were harvested on day 40 (Figure 7A). Attenuated allograft fibrosis was noted in AM095-treated allografts, with decreased peribronchial and perivascular collagen expression noted on trichrome staining (Figure 7B). The effect was found to be more pronounced in animals treated with AM095 from days 14 to 40 as compared with those treated from days 14 to 28 only. Airway wall thickness (VV_{sub}), a morphometric quantitative measure of airway remodeling, was noted to be significantly decreased in AM095-treated allografts with both durations (Figure 7C). Total collagen expression in the lungs was quantitated by

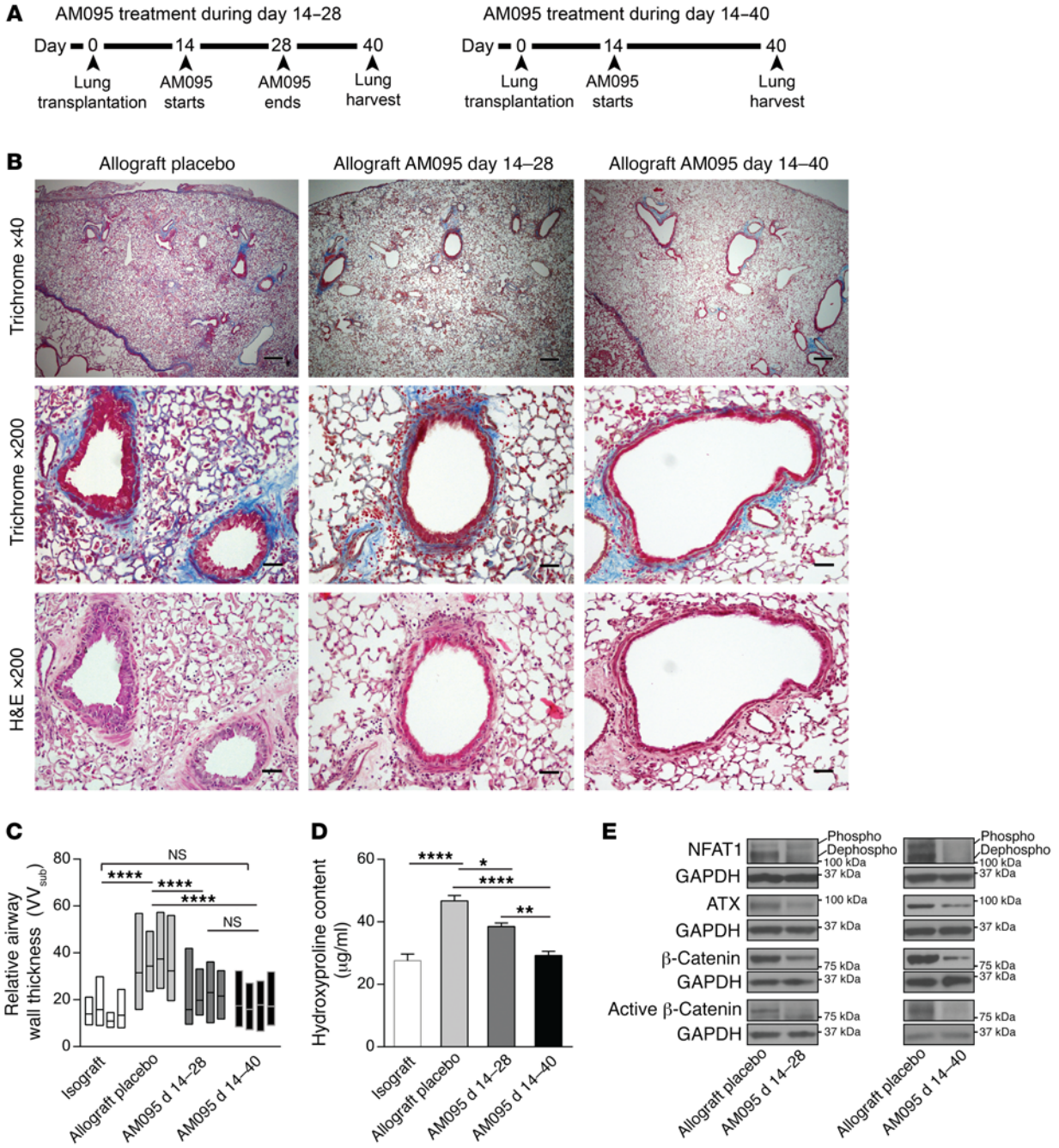

Figure 7. LPA1 antagonist AM095 treatment decreases lung allograft fibrosis in murine orthotopic lung transplant model. (**A**) Time line of two durations of AM095 treatment. (**B**) Decreased airway remodeling and fibrosis in allografts treated with AM095 by trichrome and H&E staining. Lung allografts were treated with AM095 during days 14–28 or days 14–40, both harvested on day 40 after transplantation (n = 5 for placebo, 4 for AM095 treatment during days 14–28, and 5 for AM095-treated allografts during days 14–40). An Olympus BX41 microscope with an Olympus DP20 camera was used to take images. Scale bars: 200 μm for ×40 images and 40 μm for ×200 images. (**C**) Morphometric analysis of airway wall thickness in transplanted placebo allografts, AM095-treated allografts for days 14–28, and AM095-treated allografts for days 14–40 (n = 4/group with ANOVA). Data are represented by floating bars ranging from minimum to maximum, with a line showing the mean value of each graft. (**D**) Hydroxyproline assay in lung grafts was conducted for collagen content quantitation. Both durations of AM095 treatment significantly reduced hydroxyproline content in allografts (n = 7 for isograft and 6 for the rest of the groups, with ANOVA). *P < 0.05, **P < 0.01, ****P < 0.0001. (**E**) Dephosphorylated (dephospho) NFAT1, ATX, and total and active β-catenin proteins was decreased in allografts treated with AM095 (n = 4/group) by immunoblot.

hydroxyproline assay and demonstrated significantly lower levels in allografts treated with AM095 as compared with placebo-treated allografts (Figure 7D). Collagen content of the allografts treated with AM095 from days 14 to 40 was significantly lower than that of allografts treated from days 14 to 28 only. Next, to investigate the in vivo relevance of our proposed LPA/LPA1/β-catenin and LPA/LPA1/NFAT1/ATX signaling axis to allograft fibrogenesis, we compared protein expression in whole lung allografts in the

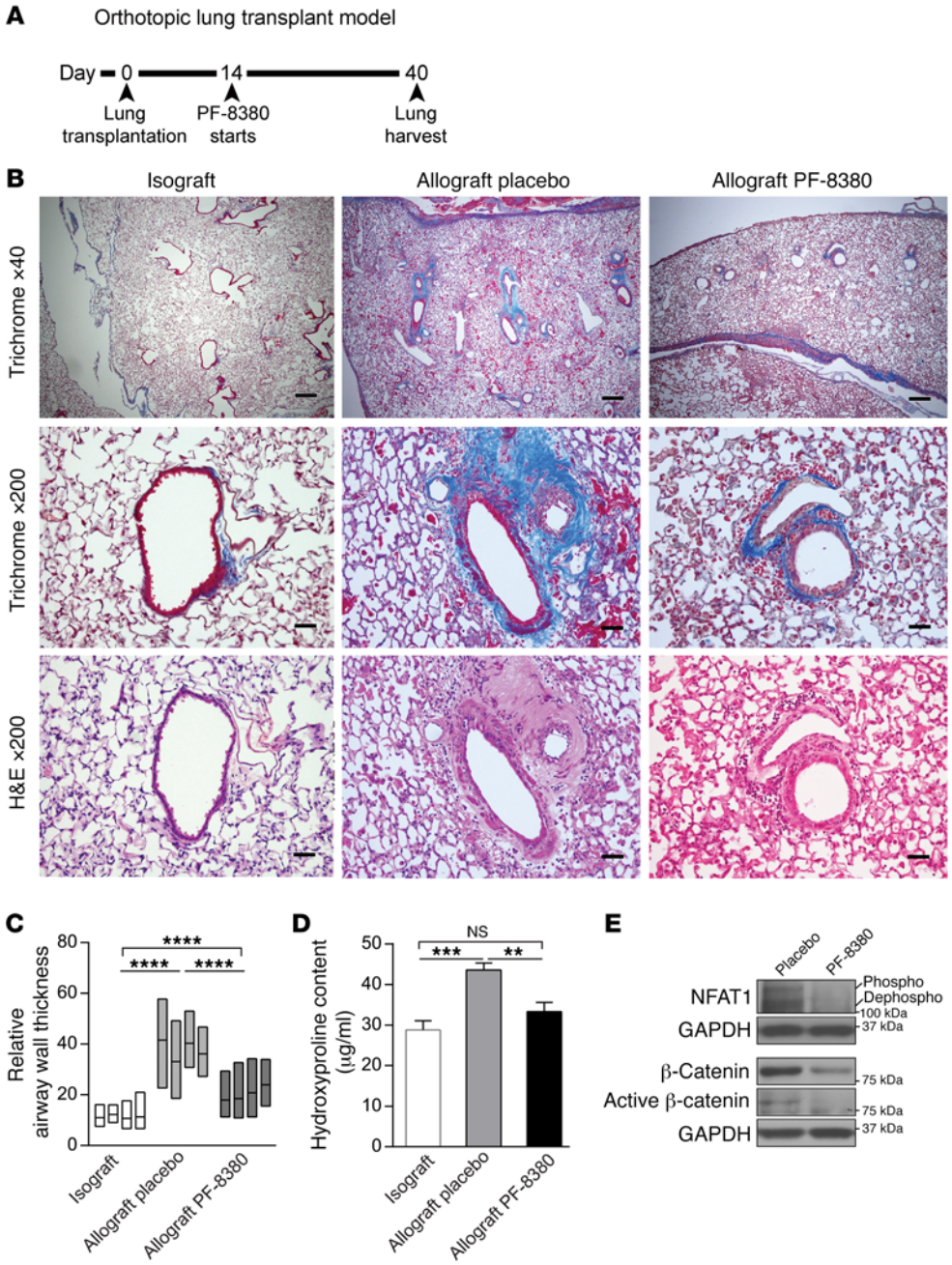

Figure 8. PF-8380 attenuates lung allograft fibrosis and BO development in murine orthotopic lung transplant model. (**A**) Time line of murine orthotopic lung transplantation and administration of the ATX inhibitor PF-8380. (**B**) Trichrome and H&E staining of lung grafts harvested on day 40 after transplantation demonstrated decreased airway remodeling and fibrosis in allografts treated with PF-8380 (n = 3 for isograft, 5 for placebo- and PF-8380–treated allograft). Images were taken by an Olympus BX41 microscope with an Olympus DP20 camera. Scale bars: 200 μm for ×40 images and 40 μm for ×200 images. (**C**) Morphometric analysis of airway wall thickness in transplanted lung isografts, placebo allografts, and PF-8380–treated allografts (n = 4/group with ANOVA). Data for each graft are represented as a floating bar ranging from minimum to maximum, with a line showing the mean value. Data for isografts and allograft placebos were obtained by measuring from different slides of the same animal groups as in Figure 7C. (**D**) Collagen content quantitation by hydroxyproline assay in lung grafts. PF-8380 treatment significantly reduced hydroxyproline content in allografts (n = 7 for isograft and 6 for the rest of the groups, with ANOVA). Samples for isograft and allograft placebo were from the same corresponding groups as in Figure 7D and were measured again together with PF-8380–treated allografts. $^{**}P < 0.01$, $^{***}P < 0.001$, $^{****}P < 0.0001$. (**E**) Western blot analysis demonstrated decreased expression of dephosphorylated NFAT1 and total and active β-catenin proteins in allografts treated with PF-8380 (n = 4/group). All representative blots shown were from the same biological samples. Total and active β-catenin were blotted simultaneously on 2 parallel gels.

presence and absence of AM095 by immunoblot analysis. Lower expression of total and active β-catenin protein pools, as well as decreased dephosphorylated NFAT1 and ATX protein expression, was noted in allografts treated with AM095 both for days 14–28 and days 14–40, compared with placebo controls (Figure 7E).

ATX inhibition abates fibrogenesis in the orthotopic lung transplant model. Next, we investigated whether an additional approach with pharmacological inhibition of ATX can also interrupt the proposed ATX/LPA/LPA1/β-catenin signaling axis and ameliorate lung allograft fibrogenesis. 4-[3-(2, 3-dihydro-2-oxo-6-benzoxazolyl)-3-oxopropyl]-(3, 5-dichlorophenyl)methyl ester-1-piperazinecarboxylic acid (PF-8380), a specific small molecule inhibitor of ATX with subnanomolar potency (31), was utilized. The pharmacokinetics of PF-8380 have been extensively studied in vivo, and it has been found to exhibit good oral availability (31); its long-term use had been demonstrated to have no toxic effects on mice (32). When administered orally at the dose of 30 mg/kg, PF-8380 has been shown to cause a greater than 95% reduction in LPA levels in both plasma and inflammatory tissue sites (31). Lung allografts (B6D2F1/J→DBA/2J) were treated with 30 mg/kg PF-8380, administered twice daily by oral gavage, from days 14 to 40 after transplantation (Figure 8A). Allografts were harvested, and plasma was collected on day 40 after transplantation. The efficacy of this dose was confirmed by measuring plasma LPA levels by ELISA and studying ATX activity in lung homogenates. An approximately 50% reduction in plasma LPA levels and significantly reduced ATX activity in allografts were noted in mice treated with PF-8380 (Supplemental Figure 2). Histologic evaluation of the allografts treated

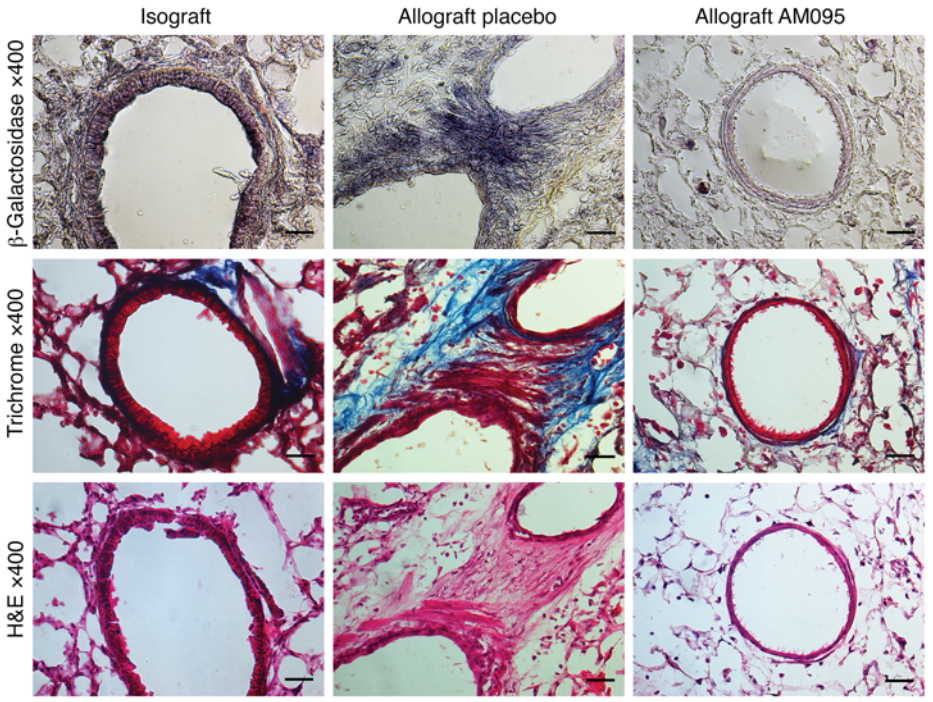

Figure 9. LPA contributes to nuclear transcriptional activity of β-catenin in vivo during allograft fibrogenesis. *Axin2*^{lacZ} mice were utilized as donors in the orthotopic lung transplant model. Transplanted mice were treated with AM095 or placebo during days 14–40 after transplantation. β-Galactosidase, trichrome, and H&E staining was performed on isografts and placebo- and AM095-treated allografts harvested at day 40 (n = 2 for isograft, n = 3 for groups of placebo- and AM095-treated allografts). Images were taken with a Nikon Eclipse E600 microscope equipped with a Cool Snap EZ camera and NIS-Elements BR3.2 software. Strong (purple) β-galactosidase staining with Salmon-gal was noted in bronchial subepithelial MCs in allografts. β-Galactosidase staining was markedly diminished in allografts treated with AM095. Scale bars: 30 μm.

with PF-8380 demonstrated decreased airway remodeling, with lower peribronchial and perivascular collagen expression noted on trichrome staining (Figure 8B) and significantly decreased VV_{sub} by morphometric analysis (Figure 8C). Hydroxyproline assay demonstrated significantly lower collagen levels in the allografts treated with PF-8380 (Figure 8D). Consistent with our proposed signaling axis, lower expression of dephosphorylated NFAT1 and of total and active β-catenin protein was noted in allografts treated with PF-8380, compared with placebo-treated controls (Figure 8E).

Role of LPA signaling in β-catenin transcriptional activation in MC in vivo during murine allograft fibrogenesis. To study the in vivo role of LPA in transcriptional activation of β-catenin during allograft fibrogenesis, we utilized *Axin2*^{lacZ} reporter mice, which carry a *lacZ* gene inserted into the *Axin2* locus, as donors in the murine orthotopic lung transplant model (33, 34). The expression of *lacZ* through the endogenous *Axin2* promoter faithfully reflects sites of β-catenin signaling, and the *Axin2*^{lacZ} mouse has been previously validated as robust and specific to detect β-catenin signaling in the lungs (35). LacZ staining of allografts on day 40 after transplantation demonstrated peribronchial lacZ expression consistent with fibrosis areas, as seen on consecutive trichrome staining slides (Figure 9). To investigate the in vivo role of LPA1 signaling in driving β-catenin transcriptional activation in MCs during allograft fibrogenesis, we treated mice that had received *Axin2*^{lacZ} donor allografts with LPA1 antagonist AM095 (30 mg/kg by oral gavage). Reduced expression of LacZ in peribronchial fibrotic areas was noted in AM095-treated mice, suggesting that LPA1 signaling plays a significant role in vivo in β-catenin activation in MCs during allograft fibrosis (Figure 9).

Discussion

A decline in lung function arising from small airway fibrosis and obliteration or BOS develops in more than 50% of human lung transplants by 5 years after transplantation and is the major cause of long-term mortality in lung transplant recipients (36). However, the mechanisms underlying fibrotic remodeling of the airways in the allograft are not well understood, and BOS represents an intractable terminal disease with few therapeutic options to prevent its development or slow its progression. Here, we utilized MCs from human lung allografts and a murine orthotopic single lung transplantation model of BO to investigate mechanism(s) of lung allograft fibrogenesis and delineate a NFAT1/ATX/LPA1/β-catenin signaling axis that regulates MC activation in an autocrine manner and contributes to lung allograft fibrogenesis (Figure 6I). Furthermore, our studies suggest a potential role for LPA1 antagonists and ATX inhibitors as therapeutic options in BOS and demonstrate the in vivo contribution of ATX/LPA1 signaling to β-catenin activation.

Our studies and data identify an autocrine mechanism of fibrotic activation in lung MCs that contributes to allograft fibrogenesis. Dysfunctional and persistent MC activation plays a key role in the progression of tissue fibrosis. β-Catenin has been demonstrated to be a key element in MC activation and fibrosis. The stably increased β-catenin expression noted in BOS MCs is consistent with previous studies of human MCs from other fibrotic conditions (11). A unique finding was that interrupting *LPA1* signaling or *ATX* expression in BOS MCs was sufficient to reverse their fibrotic state in vitro and abrogated their ability to establish fibrotic lesions after adaptive transfer in vivo. These findings demonstrate a previously unappreciated autocrine mechanism of cellular activation whereby MCs can regulate β-catenin and matrix expression via autocrine ATX secretion and downstream LPA1 signaling. Furthermore, the demonstration of a role for NFAT1 in induction of *ATX* and downstream β-catenin activation reveals links between these key regulatory pathways and provides insight into the self-perpetuating nature of fibrosis.

The role of the ATX/LPA pathway in BOS has not been previously recognized, and we believe these are the first studies to investigate this signaling pathway in lung allograft fibrogenesis. In the murine lung transplant model of BO, LPA1 antagonism and ATX inhibition were noted to be protective and associated with a significant decrease in allograft fibrosis, as demonstrated by histology and quantitative analysis of tissue collagen. This finding is of potentially significant clinical relevance, as orally available selective LPA1 antagonists have demonstrated efficacy in other murine models of tissue fibrosis (16, 37) and are in clinical trials in patients with idiopathic pulmonary fibrosis. Development of ATX inhibitors for clinical use has also received significant interest, and these compounds are being evaluated in preclinical studies (38–41). We utilize a murine lung transplant model of BO in the preclinical investigation of AM095 and PF-8380. The drugs were dosed starting on day 14, a time point beyond the initial ischemia-reperfusion phase and well into the alloimmune injury phase. In this model, in which development of BO is highly penetrant and reproducible, fibrosis is well established on day 28 and progresses further by day 40 (30). Statistically significant differences were noted on day 40 between AM095- or PF-8380–treated and placebo-treated animals, demonstrating that both drugs prevented the development and progression of fibrosis. Interestingly, treatment with AM095 for 14 days (from days 14 to 28) seems to have a residual inhibitory effect in lung allograft fibrosis when examined on day 40. However, comparison of the two groups with different treatment durations (days 14–28 and days 14–40) demonstrated that continued LPA1 antagonism leads to a much more robust decrement in allograft fibrogenesis. While pharmacologic inhibition of LPA1 or ATX in a murine model does not provide a cell type–specific approach in targeting MCs, our data demonstrate a role for inhibition of the ATX/LPA/LPA1 axis in targeting chronic allograft rejection and underscore the potential importance of this approach for future human therapeutic trials.

The present study provides what we believe to be the first in vivo evidence for the role of LPA in regulating β-catenin signaling. Lung allografts from *Axin2*^{lacZ} reporter mice were utilized to elucidate the requisite role for LPA in β-catenin transcriptional activation in vivo during allograft fibrogenesis. While β-catenin activation has long been recognized as the major effector of the Wnt signaling pathway, recent studies have suggested a role for GPCRs in activation of the β-catenin pathway (13, 14). LPA as a ligand for β-catenin activation was first noted in colon cancer cells, where β-catenin was demonstrated to be important for mediating cellular proliferation in the presence of LPA. The increase in β-catenin was shown to be dependent on LPA2 and LPA3 receptors in these cells (42). Subsequently, while investigating MC migration in lung allografts, we discovered that β-catenin is activated in MCs in the presence of LPA and is essential for LPA-induced migration in vitro (15). β-Catenin activation in lung MCs was found to be regulated via LPA1-dependent GSK-3β phosphorylation. Others have since reiterated the role for LPA in promoting β-catenin stabilization and transcriptional activation (43, 44). However, all these investigations have been performed in vitro, and whether LPA truly acts as a ligand in vivo had not been established. Lung allografts from reporter mice (*Axin2*^{lacZ}) allowed us to follow β-catenin transcriptional activity during allograft fibrogenesis and test the in vivo role of LPA1 ligation in β-catenin activation in MCs. In mice treated with the LPA1 antagonist AM095, a significant decrease in β-catenin transcriptional activation was noted, demonstrating a requisite role for LPA in β-catenin activation in this disease model.

We demonstrate that *NFAT1* regulates *ATX* transcriptional expression in MCs and that increased ATX expression in fibrotic MCs is dependent on *NFAT1* signaling. MCs from patients with BOS demonstrated an ATX-secretory function, as evidenced by increased ATX production as well as activity. This stable upregulation of ATX in cells removed from their microenvironment has also been previously demonstrated in synovial cells from patients with rheumatoid arthritis (45), as well as in human cancer cell lines (46). While ATX can be produced by a variety of cell types and ATX can be measured in biological fluids such as blood, it has been suggested that ATX expressed by cells can regulate their own local biological functions. The significance of ATX as a local regulator in the cellular niche has been strengthened by studies demonstrating that neutralization of circulating ATX is unable to affect local tissue processes (47). However, in spite of the recognition of the significant biological role of ATX, with its overexpression linked to disease pathogenesis, not much is known about regulators of *ATX* expression. While ATX expression has been shown to be induced in the inflammatory state, this has been noted to be independent of lymphoid cytokines and TLR signaling (47). NFAT binding sites are found in the *ATX* promoter, and NFAT1 has been demonstrated to bind the *ATX* promoter in breast carcinoma cells (25). We found that *NFAT1* overexpression in non-fibrotic MCs significantly upregulated *ATX* mRNA expression and increased ATX protein expression and activity. In BOS MCs, where ATX was upregulated at baseline, *NFAT1* silencing strongly decreased *ATX* expression as well as protein activity. Calcium signaling has been shown to be dysregulated in fibrotic cells (48), consistent with our finding in BOS MCs, where increased NFAT1 total and nuclear protein expression was noted. LPA as a regulator of calcium signaling was associated with NFAT1 nuclear translocation, suggesting a positive feedback that can continue to sustain this dysregulated activation cycle.

In summary, we identity a mechanism of regulation of β-catenin activation in MCs via autocrine ATX secretion. NFAT1 was identified as a key transcriptional regulator of *ATX*, and these studies are the first to our knowledge to demonstrate a link between the two key transcriptional regulators, NFAT1 and β-catenin. Additionally, we believe that this is the first investigation to demonstrate a role for LPA1 signaling in the pathogenesis of lung allograft fibrosis. The lack of effective therapies to stop BOS progression and the significant effect of AM095 and PF-8380 in the murine model of BO suggest that LPA1 antagonists and ATX inhibitors might prove to be an effective therapeutic intervention.

Methods

Cell isolation and culture conditions. Bronchoalveolar lavage from lung transplant recipients with and without evidence of BOS was utilized for MC isolation. BOS was identified based on criteria defined by International Society of Heart and Lung Transplantation guidelines and as previously described (3). Non-BOS MCs were obtained from lung transplant recipients who were BOS-free and had no evidence of acute rejection or infection with transbronchial biopsies and microbiological cultures, respectively. MCs were isolated and characterized as previous-

ly described (2). Briefly, cells isolated from bronchoalveolar lavage fluid by centrifugation (200 *g* for 5 minutes) were maintained in adherent culture conditions, and MCs were identified by their growth as fibroblastoid colony-forming units. Cells were passaged by trypsinization and maintained in culture in high-glucose DMEM (11965118, Gibco, Thermo Fisher Scientific) with 10% FBS (F2442, Sigma-Aldrich), 100 U/ml penicillin/streptomycin (15140122, Gibco), and 0.5% Fungizone (15290018, Gibco) at 37°C in humidified incubators with 5% CO_2. Cells between passages 3 and 6 were used for experiments. The mesenchymal phenotype and purity of the cells were confirmed by staining for cell surface markers by flow cytometry. MCs demonstrated uniform expression of CD44, CD73, CD105, and CD90 and lacked expression of CD45, CD31, and EPCAM (Supplemental Figure 3). Reagents used for cell treatment included 1-oleoyl LPA (62215, Cayman Chemical) and human recombinant ATX (10803, Cayman Chemical). Before reagent treatments, cells were cultured in serum-free DMEM for 24 hours till they grew to approximately 70% confluence.

Immunoblot analysis. Whole cell lysates or nuclear fractions of MCs were extracted as previously reported (15). Mouse lung allografts with AM095 or placebo control treatment were homogenized with a Tissuemiser (15-338-420, Fisher Scientific) in CelLytic MT Cell Lysis Reagent (C3228, Sigma-Aldrich) supplemented with Protease Inhibitor Cocktail (P8340, Sigma-Aldrich) and Halt Phosphatase Inhibitor Cocktail (78426, Thermo Fisher Scientific). Then allograft homogenate was centrifuged at 4,000 *g* for 15 minutes and 17,000 *g* for 10 minutes at 4°C. Supernatants were collected, and protein concentration was determined with a Pierce Coomassie Plus (Bradford) Assay Kit (23236, Thermo Fisher Scientific) and a Thermo Scientific BioMate 3 Spectrophotometer. Western blotting was performed to analyze protein expression levels using primary antibodies against LPA1 (ab23698, Abcam, 1:200), human-specific NFAT1 (MAB6499, R&D Systems, 1:1,000), NFAT1 (MA1-025, Thermo Fisher Scientific, 1:1,000), ATX (10005375, Cayman Chemical, 1:100), β-catenin (ab6302, Abcam, 1:2,000), active β-catenin (05-665, Millipore, 1:1,000), phospho–GSK-3β (ab75814, Abcam, 1:500), collagen I (CL50111AP-1, Cedarlane, 1:500), GAPDH (MAB374, Millipore, 1:5,000), and SAM68 (sc-333, Santa Cruz Biotechnology Inc., 1:1,000). HRP-conjugated anti-mouse and anti-rabbit secondary antibodies were A8924 (Sigma-Aldrich, 1:20,000) and A0545 (Sigma-Aldrich, 1:10,000), respectively.

Gene silencing. For siRNA, MCs were transiently transfected at 60%–70% confluence with 100 nM siRNA targeting β-catenin (42816, Ambion), *NFAT1* (M-003606-02-0005, Dharmacon), *LPA1* (4050, Ambion), *ATX* (M-004601-02-0005, Dharmacon), and nontargeting scrambled siRNA (sc-37007, Santa Cruz Biotechnology Inc.) using Oligofectamine (12252-011, Invitrogen) in Opti-MEM I reduced serum medium overnight. Then MCs were cultured in serum-free DMEM for another 48 hours before any additional treatment or 72 hours before harvesting of cells for protein or RNA isolation. To silence *ATX* and *LPA1* by shRNA, respectively, for adoptive transfer, DsRed-labeled MCs were infected with MISSION Lentiviral Transduction Particles (SHCLNV, Sigma-Aldrich) containing either a shRNA targeting *ATX* or *LPA1* or with control silencing vector pLKO.1. The sequences of *ATX* or *LPA1* shRNA constructs within the pLKO.1 vector were 5′-CCGGGCTCCTAATAATGGGACCCATCTCGAGATGGGTCCCATTATTAGGAGCTTTTTG-3′ and 5′-GGTTGCAATCGAGAGGCACATTACTCGAGTAATGTGCCTCTCGATTGCAATTTTTG-3′, respectively.

Immunohistochemical staining of human BO lesions. Immunohistochemistry staining was performed on human lung BO lesions in autopsy samples according to standard clinical laboratory procedures. Primary antibodies for β-catenin (ab6302, Abcam, 1:1,000), ATX (H-008-29, Phoenix Pharmaceuticals, 1:1,000), and α-SMA (ab124964, Abcam, 1:500) were used in this study. Imaging was performed with an Olympus BX41 microscope connected to an Olympus DP20 camera.

ATX ELISA and ATX activity assay. BOS and Non-BOS cell lines were cultured in 60-mm dishes until confluent. Cells were washed once with PBS and then serum starved for 24 hours. Serum-free supernatant was collected, and ATX levels were measured with a Human ENPP-2/Autotaxin Quantikine ELISA Kit (DENP20, R&D Systems) according to the manufacturer's protocol. Absorbance at 450 nm was measured using a SpectraMax M3 multi-mode microplate reader (Molecular Devices). For ATX activity, cell supernatant was collected, centrifuged at 17,000 *g* for 10 minutes at 4°C to sediment floating cells or debris, and concentrated to one-eighth of the original volume with an Amicon Ultra-4 Centrifugal Filter Unit with Ultracel-3 membrane (UFC800308, EMD Millipore). After measurement of protein concentration, an equal amount of total protein was subjected to ATX activity assay with the fluorogenic phospholipid ATX substrate FS-3 (L-2000, Echelon) (49, 50). Briefly, 30 μl supernatant and 40 μl FS-3 solution (containing 5 μM FS-3, 140 mM NaCl, 5 mM KCl, 1 mM $CaCl_2$, 1 mM $MgCl_2$, 50 mM Tris-HCl pH 8.0, and 1 mg/ml BSA) were mixed and loaded to a Costar 96-well black-wall, clear-bottom plate. Fluorescence of samples was measured using a SpectraMax M3 multi-mode microplate reader (Molecular Devices) at excitation and emission wavelengths of 485 nm and 528 nm, respectively.

For ATX activity assays in lung lysates, 20 μl allograft lysate and 40 μl FS-3 solution were mixed, and ATX activity was measured similarly for placebo- and PF-8380–treated lung allografts.

RNA isolation and real-time PCR. Total RNA was isolated using the RNeasy Mini Kit (74104, QIAGEN), and cDNA was synthesized with the High Capacity cDNA reverse transcription kit (4368814, Applied Biosystems). Real-time PCR for *ATX*, *Axin2*, *NFAT1*, *LPA1*, and β-actin was conducted with probes Hs00905125_m1, Hs_00610344_m1, Hs00905451_m1, Hs_00173500_m1, and 4310881E (Applied Biosystems), respectively, and TaqMan Gene Expression Master Mix (4369016, Applied Biosystems). Real-time PCR for *COL1A1* transcripts was conducted in SYBR Green PCR Master Mix (4309155, Applied Biosystems) and with the following primers: COL1A1F, GTGCGATGACGTGATCTGTGA and COL1A1R, CGGTGGTTTCTTGGTCGGT. The relative mRNA levels of the target genes were calculated as equal to $2^{-(\Delta Ct\ target\ mRNA\ -\ \Delta Ct\ \beta\text{-}actin)}$.

GFP-NFAT1 subcellular localization by live cell imaging. Plasmid for expressing GFP-NFAT1 fusion protein was provided by Jaime Modiano of the University of Minnesota, Minneapolis, Minnesota, USA (51). Non-BOS MCs were transfected with GFP-NFAT1–expressing plasmid using Lipofectamine LTX reagent (94756, Invitrogen) and Plus reagent (10964-021, Invitrogen) according to the manufacturer's instructions. Stable clones of cells expressing GFP-NFAT1 were selected in complete DMEM supplemented with 150 μg ml^{-1} G418 sulfate (10131-035, Gibco) and maintained in 100 μg ml^{-1} G418-containing medium. GFP-NFAT1 localization and nucleus staining by Hoechst 33342 (62249, Thermo Scientific) in live cells were examined using a Nikon Eclipse TE2000-E microscope equipped with a Cool Snap HQ^2 camera operated with the Metamorph program.

Murine orthotopic lung transplantation model and β-galactosidase staining. Orthotopic left lung transplantations were performed using a previously described technique (30). Male mice aged 8–12 weeks and weighing 24–30 g were used as donors or recipients. Isografts were performed in the B6D2F1/J lungs→B6D2F1/J strain combinations, and allogeneic transplants were performed in the B6D2F1/J lungs→DBA/2J strain combinations. A surgical microscope (SZX16-SZX2; Olympus) with ×2.1 to ×34.5 magnifications was used for all procedures. Buprenorphine was given to recipient mice at the conclusion of the procedure and again every 12 hours until 3 days after transplant. Morphometric analysis and hydroxyproline quantification were performed as described previously (30). For β-catenin transcriptional activity assays, *Axin2*^{lacZ} mice of B6D2F1/J was generated by crossing C57BL/6 *Axin2*^{lacZ} (B6.129P2-*Axin2*^{tm1Wbm}/J, stock 009120, The Jackson Laboratory) females with DBA/2J males. For β-galactosidase staining, sections were incubated in staining solution: 1 mg/ml Salmon-gal (6-chloro-3-indolyl-β-D-galactopyranoside) (X668, Lab Scientific) and 0.4 mM NBT (4-nitro blue tetrazolium chloride) (11383213001, Roche) in PBS at 37°C for 3 hours (52).

Oral gavage. Oral gavage was performed in a containment room of the University of Michigan animal facility. PF-8380 (HY-13344, MedChem Express) and AM095 were dissolved in PEG 400 at a concentration of 6 mg/ml. Body weights of animals were measured daily. Treatment with PF-8380 or AM095 was administered by oral gavage twice daily at a dosage of 30 mg/kg body weight starting from day 14 after lung transplantation. Placebo-treated mice were given vehicle (PEG 400) via oral gavage ingestion. On day 40 after lung transplantation, mice were sacrificed, and lung allografts were harvested for Western blotting, hydroxyproline assay, or immunohistochemistry.

Statistics. Statistical significance was analyzed using GraphPad Prism 6 Software. Data are presented as mean values ± SEM unless otherwise noted. Significance was assessed with Student's *t* test for comparisons of 2 groups, or with ANOVA and a post hoc Bonferroni test for 3 or more groups. *P* values less than 0.05 were considered significant.

Study approval. Written informed consent was received from lung transplant recipient participants included in the study. Human lung-resident MCs from bronchoalveolar lavage were isolated under a protocol approved by the Institutional Review Board of the University of Michigan. Mouse experiments were performed according to IACUC-approved protocols at the University of Michigan.

Author contributions

PC, LB, NMW, ERF, and VNL conceptualized and designed research studies; PC, YA, LB, NMW, CMM, AL, ERF, and VNL conducted experiments and acquired, analyzed, and interpreted data; VNL and ERF provided reagents; VNL, PC, and ERF wrote the manuscript.

Acknowledgments

This study was supported by NIH grants R01 HL118017 and R01 HL094622 (awarded to VNL), a Scleroderma Research Foundation Award, the Brian and Mary Campbell and Elizabeth Campbell Carr Research Gift Fund (to VNL), and a Ruth L. Kirschstein National Research Service Award (5T32HL007749 to PC). AM095 was a gift from Bristol-Myers Squibb.

Address correspondence to: Vibha N. Lama, Division of Pulmonary and Critical Care Medicine, Department of Internal Medicine, University of Michigan Health System, 1500 W Medical Center Drive, 3916 Taubman Center, Ann Arbor, Michigan 48109-0360, USA. Phone: 734.936.5047; E-mail: vlama@umich.edu.

1. Estenne M, et al. Bronchiolitis obliterans syndrome 2001: an update of the diagnostic criteria. *J Heart Lung Transplant*. 2002;21(3):297–310.
2. Lama VN, et al. Evidence for tissue-resident mesenchymal stem cells in human adult lung from studies of transplanted allografts. *J Clin Invest*. 2007;117(4):989–996.
3. Badri L, et al. Mesenchymal stromal cells in bronchoalveolar lavage as predictors of bronchiolitis obliterans syndrome. *Am J Respir Crit Care Med*. 2011;183(8):1062–1070.
4. Walker N, et al. Resident tissue-specific mesenchymal progenitor cells contribute to fibrogenesis in human lung allografts. *Am J Pathol*. 2011;178(6):2461–2469.
5. Li Y, et al. Severe lung fibrosis requires an invasive fibroblast phenotype regulated by hyaluronan and CD44. *J Exp Med*. 2011;208(7):1459–1471.
6. Wynn TA, Ramalingam TR. Mechanisms of fibrosis: therapeutic translation for fibrotic disease. *Nat Med*. 2012;18(7):1028–1040.
7. Caplan AI, Dennis JE. Mesenchymal stem cells as trophic mediators. *J Cell Biochem*. 2006;98(5):1076–1084.
8. Cheon S, et al. Prolonged beta-catenin stabilization and tcf-dependent transcriptional activation in hyperplastic cutaneous wounds. *Lab Invest*. 2005;85(3):416–425.
9. Cheon SS, et al. beta-Catenin stabilization dysregulates mesenchymal cell proliferation, motility, and invasiveness and causes aggressive fibromatosis and hyperplastic cutaneous wounds. *Proc Natl Acad Sci USA*. 2002;99(10):6973–6978.
10. Lam AP, et al. Nuclear β-catenin is increased in systemic sclerosis pulmonary fibrosis and promotes lung fibroblast migration and proliferation. *Am J Respir Cell Mol Biol*. 2011;45(5):915–922.
11. Lam AP, Gottardi CJ. β-catenin signaling: a novel mediator of fibrosis and potential therapeutic target. *Curr Opin Rheumatol*. 2011;23(6):562–567.
12. Wei J, et al. Canonical Wnt signaling induces skin fibrosis and subcutaneous lipoatrophy: a novel mouse model for scleroderma? *Arthritis Rheum*. 2011;63(6):1707–1717.
13. Jin T, George Fantus I, Sun J. Wnt and beyond Wnt: multiple mechanisms control the transcriptional property of beta-catenin. *Cell Signal*. 2008;20(10):1697–1704.
14. Shevtsov SP, Haq S, Force T. Activation of beta-catenin signaling pathways by classical G-protein-coupled receptors: mechanisms and consequences in cycling and non-cycling cells. *Cell Cycle*. 2006;5(20):2295–2300.
15. Badri L, Lama VN. Lysophosphatidic acid induces migration of human lung-resident mesenchymal stem cells through the β-catenin pathway. *Stem Cells*. 2012;30(9):2010–2019.
16. Castelino FV, et al. Amelioration of dermal fibrosis by genetic deletion or pharmacologic antagonism of lysophosphatidic acid receptor 1 in a mouse model of scleroderma. *Arthritis Rheum*. 2011;63(5):1405–1415.
17. Pradère JP, et al. Lysophosphatidic acid and renal fibrosis. *Biochim Biophys Acta*. 2008;1781(9):582–587.
18. Pradère JP, et al. LPA1 receptor activation promotes renal interstitial fibrosis. *J Am Soc Nephrol*. 2007;18(12):3110–3118.
19. Tager AM, et al. The lysophosphatidic acid receptor LPA1 links pulmonary fibrosis to lung injury by mediating fibroblast recruitment and vascular leak. *Nat Med*. 2008;14(1):45–54.
20. Bullions LC, Levine AJ. The role of beta-catenin in cell adhesion, signal transduction, and cancer. *Curr Opin Oncol*. 1998;10(1):81–87.
21. Moolenaar WH. Development of our current understanding of bioactive lysophospholipids. *Ann N Y Acad Sci*. 2000;905:1–10.
22. Rivera R, Chun J. Biological effects of lysophospholipids. *Rev Physiol Biochem Pharmacol*. 2008;160:25–46.
23. Badri L, et al. Epithelial interactions and local engraftment of lung-resident mesenchymal stem cells. *Am J Respir Cell Mol Biol*. 2011;45(4):809–816.
24. Pierce EM, et al. Therapeutic targeting of CC ligand 21 or CC chemokine receptor 7 abrogates pulmonary fibrosis induced by the

adoptive transfer of human pulmonary fibroblasts to immunodeficient mice. *Am J Pathol*. 2007;170(4):1152–1164.
25. Chen M, O'Connor KL. Integrin alpha6beta4 promotes expression of autotaxin/ENPP2 autocrine motility factor in breast carcinoma cells. *Oncogene*. 2005;24(32):5125–5130.
26. van Meeteren LA, Moolenaar WH. Regulation and biological activities of the autotaxin-LPA axis. *Prog Lipid Res*. 2007;46(2):145–160.
27. Lapierre DM, et al. Lysophosphatidic acid signals through multiple receptors in osteoclasts to elevate cytosolic calcium concentration, evoke retraction, and promote cell survival. *J Biol Chem*. 2010;285(33):25792–25801.
28. Meyer Zu Heringdorf D. Lysophospholipid receptor-dependent and -independent calcium signaling. *J Cell Biochem*. 2004;92(5):937–948.
29. Sun R, et al. Different effects of lysophosphatidic acid on L-type calcium current in neonatal rat ventricular myocytes with and without H_2O_2 treatment. *Prostaglandins Other Lipid Mediat*. 2015;118–119:1–10.
30. Mimura T, et al. Local origin of mesenchymal cells in a murine orthotopic lung transplantation model of bronchiolitis obliterans. *Am J Pathol*. 2015;185(6):1564–1574.
31. Gierse J, et al. A novel autotaxin inhibitor reduces lysophosphatidic acid levels in plasma and the site of inflammation. *J Pharmacol Exp Ther*. 2010;334(1):310–317.
32. Katsifa A, et al. The bulk of autotaxin activity is dispensable for adult mouse life. *PLoS One*. 2015;10(11):e0143083.
33. Leung JY, et al. Activation of AXIN2 expression by beta-catenin-T cell factor. A feedback repressor pathway regulating Wnt signaling. *J Biol Chem*. 2002;277(24):21657–21665.
34. Lustig B, et al. Negative feedback loop of Wnt signaling through upregulation of conductin/axin2 in colorectal and liver tumors. *Mol Cell Biol*. 2002;22(4):1184–1193.
35. Al Alam D, et al. Contrasting expression of canonical Wnt signaling reporters TOPGAL, BATGAL and Axin2(LacZ) during murine lung development and repair. *PLoS One*. 2011;6(8):e23139.
36. Christie JD, et al. The Registry of the International Society for Heart and Lung Transplantation: 29th adult lung and heart-lung transplant report-2012. *J Heart Lung Transplant*. 2012;31(10):1073–1086.
37. Swaney JS, et al. Pharmacokinetic and pharmacodynamic characterization of an oral lysophosphatidic acid type 1 receptor-selective antagonist. *J Pharmacol Exp Ther*. 2011;336(3):693–700.
38. Castagna D, Budd DC, Macdonald SJ, Jamieson C, Watson AJ. Development of autotaxin inhibitors: an overview of the patent and primary literature. *J Med Chem*. 2016;59(12):5604–5621.
39. Schleicher SM, et al. Autotaxin and LPA receptors represent potential molecular targets for the radiosensitization of murine glioma through effects on tumor vasculature. *PLoS One*. 2011;6(7):e22182.
40. Benesch MG, Tang X, Venkatraman G, Bekele RT, Brindley DN. Recent advances in targeting the autotaxin-lysophosphatidate-lipid phosphate phosphatase axis in vivo. *J Biomed Res*. 2016;30(4):272–284.
41. Tager AM. Autotaxin emerges as a therapeutic target for idiopathic pulmonary fibrosis: limiting fibrosis by limiting lysophosphatidic acid synthesis. *Am J Respir Cell Mol Biol*. 2012;47(5):563–565.
42. Yang M, et al. G protein-coupled lysophosphatidic acid receptors stimulate proliferation of colon cancer cells through the {beta}-catenin pathway. *Proc Natl Acad Sci USA*. 2005;102(17):6027–6032.
43. Burkhalter RJ, Westfall SD, Liu Y, Stack MS. Lysophosphatidic acid initiates epithelial to mesenchymal transition and induces β-catenin-mediated transcription in epithelial ovarian carcinoma. *J Biol Chem*. 2015;290(36):22143–22154.
44. Ryu JM, Han HJ. Autotaxin-LPA axis regulates hMSC migration by adherent junction disruption and cytoskeletal rearrangement via LPAR1/3-dependent PKC/GSK3β/β-catenin and PKC/Rho GTPase pathways. *Stem Cells*. 2015;33(3):819–832.
45. Nikitopoulou I, et al. Autotaxin expression from synovial fibroblasts is essential for the pathogenesis of modeled arthritis. *J Exp Med*. 2012;209(5):925–933.
46. Houben AJ, Moolenaar WH. Autotaxin and LPA receptor signaling in cancer. *Cancer Metastasis Rev*. 2011;30(3-4):557–565.
47. Nakasaki T, et al. Involvement of the lysophosphatidic acid-generating enzyme autotaxin in lymphocyte-endothelial cell interactions. *Am J Pathol*. 2008;173(5):1566–1576.
48. Rahaman SO, et al. TRPV4 mediates myofibroblast differentiation and pulmonary fibrosis in mice. *J Clin Invest*. 2014;124(12):5225–5238.
49. Ferguson CG, Bigman CS, Richardson RD, van Meeteren LA, Moolenaar WH, Prestwich GD. Fluorogenic phospholipid substrate to detect lysophospholipase D/autotaxin activity. *Org Lett*. 2006;8(10):2023–2026.
50. Gaetano CG, Samadi N, Tomsig JL, Macdonald TL, Lynch KR, Brindley DN. Inhibition of autotaxin production or activity blocks lysophosphatidylcholine-induced migration of human breast cancer and melanoma cells. *Mol Carcinog*. 2009;48(9):801–809.
51. Frazer-Abel AA, et al. Nicotine activates nuclear factor of activated T cells c2 (NFATc2) and prevents cell cycle entry in T cells. *J Pharmacol Exp Ther*. 2004;311(2):758–769.
52. Sundararajan S, Wakamiya M, Behringer RR, Rivera-Pérez JA. A fast and sensitive alternative for β-galactosidase detection in mouse embryos. *Development*. 2012;139(23):4484–4490.